

Chapter 5

The three-degree-of-freedom planar parallel manipulator

5.1 Introduction

As an extension to the work presented in the previous chapter, the constrained optimization formulations presented here are aimed at determining 3-dof planar parallel manipulator designs so that a prescribed workspace is fully enclosed and well-conditioned with respect to some performance index. Depending on the particular application, certain manipulator performance criteria may be of more importance than others (see Section 1.4.1). The performance measure used here is the condition number of the manipulator Jacobian matrix, although a number of other performance measures, or a combination of such measures, could also have been used. The optimization method used in performing the optimization is the Dynamic-Q method.

In the next two sections the 3-*RPR* planar parallel manipulator, and the kinematics and determination of the condition number for this manipulator, are presented. The remainder of this chapter then separately deals with the

topics of workspace determination and dimensional synthesis of 3-dof parallel manipulators. In Sections 5.4 and 5.5 the chord workspace determination methodology is extended to the determination of constant orientation and dextrous workspaces of planar 3- RPR manipulators.

The P synthesis methodology developed in Chapter 4 is then applied to the 3-dof planar manipulator. Three forms of the dimensional synthesis problem are proposed and implemented. These forms differ from each other in the way that the orientational ability of the 3-dof platform is accounted for. Respectively, the dimensional synthesis is performed for a *single constant orientation* workspace (SO synthesis), *multiple constant orientation* workspaces (MO synthesis), and for a *dextrous* workspace (D synthesis). These methodologies and are discussed in Sections 5.6 to 5.8.

5.2 The three-degree-of-freedom parallel manipulator

The manipulator considered in this chapter is the 3-dof planar parallel mechanism shown in Figure 5.1. The manipulator consists of a platform of length $2r$ connected to a base by three linear actuators, which control the three output degrees of freedom of the platform. The actuators have leg lengths l_1 , l_2 and l_3 and are joined to the base and platform by means of revolute joints identified by the letters $A - E$. It will be assumed that $y_C = y_D = y_E$. The coordinates of point P , the mid-point of the platform, are (x_P, y_P) and the orientation of the platform is ϕ_P . With reference to the definitions given in Section 4.2, the actuator leg lengths are the input variables, i.e. $\mathbf{v} = [l_1, l_2, l_3]^T \in \mathfrak{R}^3$. The global coordinates of the working point P form the output coordinates, i.e. $\mathbf{u} = [x_P, y_P]^T \in \mathfrak{R}^2$. In contrast with the 2-dof manipulator considered in the previous chapter, the 3-dof manipulator may, in addition to positioning P in the $x - y$ plane, be orientated at an angle ϕ_P by controlling the three

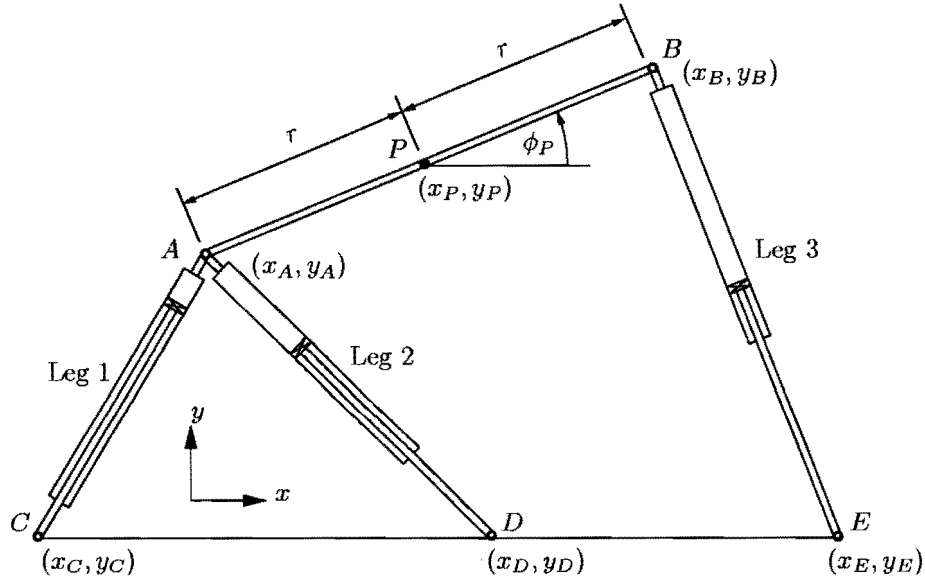


Figure 5.1: The 3-dof parallel manipulator

leg lengths. It is evident that this manipulator thus has three degrees of freedom. The rotation angle of the platform is considered as an intermediate coordinate $w = \phi_P$. For the 3-dof manipulator $nu = 2$, $nv = 3$ and $nw = 1$. The generalized coordinates for this platform are therefore given by

$$\mathbf{q} = [\mathbf{u}^\top, \mathbf{v}^\top, w]^\top = [x_P, y_P, l_1, l_2, l_3, \phi_P]^\top \in \mathbb{R}^6 \quad (5.1)$$

In the vicinity of an assembled configuration the input, output and intermediate coordinates satisfy the m independent kinematic constraint equations of the form

$$\Phi(\mathbf{q}) = \Phi(\mathbf{u}, \mathbf{v}, w) = \mathbf{0} \quad (5.2)$$

For the 3-dof planar parallel manipulator, $m = 3$.

In general, factors imposed by the physical construction of the planar parallel manipulator, which limit the workspace, may be related to the input variables or a combination of input, output and intermediate variables. An example of former type for the planar parallel manipulator are leg length limits, and of the latter, limits on the angular displacement of the revolute

joints connecting the legs to the ground and to the platform. These limiting factors are described by means of inequality constraints and may respectively take the general forms

$$\mathbf{v}^{\min} \leq \mathbf{v} \leq \mathbf{v}^{\max} \quad (5.3)$$

$$\mathbf{g}^{\min} \leq \mathbf{g}(\mathbf{u}, \mathbf{v}, w) \leq \mathbf{g}^{\max} \quad (5.4)$$

Limits on the platform orientation (intermediate coordinate) take one of two forms given by

$$w^{\min} \leq w \leq w^{\max} \quad (5.5)$$

$$\text{or } w = w^{\text{fix}} \quad (5.6)$$

where w^{fix} is a prescribed fixed scalar quantity.

The above definitions are necessary in order to facilitate the mathematical description of kinematics and workspaces types of the 3-dof planar parallel manipulator.

5.3 The kinematics and condition number of the manipulator

In general, the parallel manipulator inverse kinematics are easy to solve. For the manipulator under consideration, the three leg lengths are given by

$$\begin{aligned} l_1^2 &= (x_P - r \cos \phi_P - x_C)^2 + (y_P - r \sin \phi_P - y_C)^2 \\ l_2^2 &= (x_P - r \cos \phi_P - x_D)^2 + (y_P - r \sin \phi_P - y_D)^2 \\ l_3^2 &= (x_P + r \cos \phi_P - x_E)^2 + (y_P + r \sin \phi_P - y_E)^2 \end{aligned} \quad (5.7)$$

Writing in the standard form of the kinematic constraint equations (5.2) and using the coordinates definitions from the previous section, (5.7) become

$$\begin{aligned} \Phi(\mathbf{u}, \mathbf{v}, w) &= \begin{bmatrix} v_1^2 - (u_1 - r \cos w - x_C)^2 - (u_2 - r \sin w - y_C)^2 \\ v_2^2 - (u_1 - r \cos w - x_D)^2 - (u_2 - r \sin w - y_D)^2 \\ v_3^2 - (u_1 + r \cos w - x_E)^2 - (u_2 + r \sin w - y_E)^2 \end{bmatrix} \\ &= \mathbf{0} \end{aligned} \quad (5.8)$$

The explicit expressions for \mathbf{v} in terms of \mathbf{u} and w , $\mathbf{v} = \mathbf{v}(\mathbf{u}, w)$, may be determined from (5.7), allowing constraints (5.3) to be written as follows:

$$\mathbf{v}^{\min} \leq \mathbf{v}(\mathbf{u}, w) \leq \mathbf{v}^{\max} \quad (5.9)$$

where $\mathbf{v}^{\min} = [l_1^{\min}, l_2^{\min}, l_3^{\min}]^T$ and $\mathbf{v}^{\max} = [l_1^{\max}, l_2^{\max}, l_3^{\max}]^T$.

As in Chapter 4, the specific performance used here to characterize the performance of the 3-dof planar parallel manipulator is the inverse of the condition number of the Jacobian matrix of the manipulator. The accuracy of control of the manipulator is dependent on the condition number, denoted here by κ . Since κ tends to infinity as the manipulator approaches a singular position, maximizing the inverse condition number, κ^{-1} , also ensures that the manipulator remains far away from singular positions. From (5.2), an inverse transformation relating the input, output and intermediate velocities can be determined:

$$\mathbf{J}_\theta \dot{\boldsymbol{\theta}} = -\mathbf{J}_v \dot{\mathbf{v}} \quad (5.10)$$

where $\boldsymbol{\theta} = [\mathbf{u}^T, w]^T$, and \mathbf{J}_θ and \mathbf{J}_v are the respective constraint Jacobian matrices containing the partial derivatives of the m kinematic constraints (5.2) with respect to the variables $\boldsymbol{\theta}$ and \mathbf{v} . Equation (5.10) can be rewritten as

$$\mathbf{J} \dot{\boldsymbol{\theta}} = \dot{\mathbf{v}} \quad (5.11)$$

where $\mathbf{J} = -\mathbf{J}_v^{-1} \mathbf{J}_\theta$. Recall that for the parallel manipulator studied here $m = n = nv = nu + nw$.

One point now arises due to the platform's orientational ability. In contrast to the the 2-dof case, the Jacobian of the manipulator contains entries related to both positional and rotational abilities of the platform. The condition number will thus inherently contain a mix of these terms. It is important to normalize the positional terms of the Jacobian matrix so that positional and rotational abilities are equally represented by the condition number. Pittens and Podhorodeski [71] and Stoughton and Arai [78] note this occurrence and suggest that the best approach is to normalize the positional terms of the Jacobian with respect to the platform radius r , a suggestion which is adopted here.

In explicit terms, differentiation, with respect to time, of the kinematic constraints (5.2), and writing in the form (5.10) yields

$$\begin{bmatrix} x_{AC} & y_{AC} & rx_{AC} \sin w - ry_{AC} \cos w \\ x_{AD} & y_{AD} & rx_{AD} \sin w - ry_{AD} \cos w \\ x_{BE} & y_{BE} & -rx_{BE} \sin w + ry_{BE} \cos w \end{bmatrix} \begin{bmatrix} \dot{u}_1 \\ \dot{u}_2 \\ \dot{w} \end{bmatrix} = \begin{bmatrix} v_1 & 0 & 0 \\ 0 & v_2 & 0 \\ 0 & 0 & v_3 \end{bmatrix} \begin{bmatrix} \dot{v}_1 \\ \dot{v}_2 \\ \dot{v}_3 \end{bmatrix} \quad (5.12)$$

where the notation $x_{AB} = x_A - x_B$ is used, and $x_A = u_1 - r \cos w$, $y_A = u_2 - r \sin w$, $x_B = u_1 + r \cos w$ and $y_B = u_2 + r \sin w$.

The Jacobian \mathbf{J} of the 3-dof planar manipulator, as defined by (5.11), is thus given by

$$\mathbf{J} = \begin{bmatrix} x_{AC}/rv_1 & y_{AC}/rv_1 & (rx_{AC} \sin w - ry_{AC} \cos w)/v_1 \\ x_{AD}/rv_2 & y_{AD}/rv_2 & (rx_{AD} \sin w - ry_{AD} \cos w)/v_2 \\ x_{BE}/rv_3 & y_{BE}/rv_3 & (-rx_{BE} \sin w + ry_{BE} \cos w)/v_3 \end{bmatrix} \quad (5.13)$$

Note the normalization of the positional terms in the first two columns by the platform radius r . The condition number κ of this 3×3 Jacobian may be determined using equations (4.19) and (4.20) of Section 4.7.2.

5.4 Constant orientation workspace determination

5.4.1 Workspace definition

The constant orientation workspace associated with a fixed value $w = w^{\text{fix}}$ of the intermediate variable, in the form of (5.6), is denoted $W^C[w^{\text{fix}}]$. In agreement with the definition given in Section 1.3.1, the constant orientation workspace of the 3-dof manipulator can be defined mathematically as

$$W^C[w^{\text{fix}}] = \{\mathbf{u} \in \mathfrak{R}^{nu} : \Phi(\mathbf{u}, \mathbf{v}, w) = \mathbf{0}, \text{ with } \mathbf{v} \text{ satisfying (5.3), (5.14)} \\ \mathbf{g}(\mathbf{u}, \mathbf{v}, w) \text{ satisfying (5.4) and } w \text{ satisfying (5.6)}\}$$

Intuitively the boundary $\partial W^C[w^{\text{fix}}]$ of the constant orientation workspace may be defined as

$$\partial W^C[w^{\text{fix}}] = \{\mathbf{u} \in \mathfrak{R}^{nu} : \mathbf{u} \in W^C[w^{\text{fix}}] \text{ and } \exists \text{ an } \mathbf{s} \in \mathfrak{R}^{nu} \text{ such that for} \\ \mathbf{u}' = \mathbf{u} + \lambda \mathbf{s}, \lambda \in \mathfrak{R} \text{ arbitrarily small and either} \\ \text{positive or negative, no } \mathbf{v} \text{ exists that satisfies (5.15)} \\ \Phi(\mathbf{u}', \mathbf{v}, w) = \mathbf{0}; \text{ as well as inequalities (5.3) and (5.4),} \\ \text{and equality constraint (5.6)}\}$$

5.4.2 Mapping the constant orientation workspace boundary

The boundary of the constant orientation workspace may be mapped numerically by means of the chord method. The basic methodology remains the

same as described in Appendix C, however the precise optimization problems used to determine points on the workspace boundary, differ for two reasons from those given by (C.9) and (C.12).

The first reason for the difference is that it has been noted that the optimization problems, used to determine successive points on the workspace boundary, can be solved much more efficiently by reducing the number of optimization variables. In the original form of both the ray and chord methods for maximal workspace determination, the output and intermediate coordinates of the manipulator were the optimization variables. For planar parallel manipulators, the resulting optimization problems thus contained *three* variables, and *one* equality constraint dictating the direction in which the next boundary point was determined. It is possible, however, to enforce the equality constraint explicitly and analytically in the optimization problem, resulting in a reduction by one of the number of required optimization variables. The resulting increase in efficiency is a result both of this, and the elimination of the numerical equality constraint and associated equality gradient function evaluations.

The second reason for the different form of the optimization problems, of course, is that the platform orientation (the intermediate coordinate) is now fixed for the constant orientation workspace. This again reduces the number of optimization variables by one, since this requirement can also be explicitly and analytically enforced in the optimization problem.

For these reasons, the precise forms of optimization problems (C.9) and (C.12) for constant orientation workspace determination are as follows. Given a radiating point \mathbf{u}^0 inside the constant orientation workspace $W^C[w^{\text{fix}}]$, and a search direction specified by a unit vector $\mathbf{s}^1 \in \mathbb{R}^2$, the output coordinates \mathbf{u} in terms of a scalar r is given by

$$\mathbf{u}(r) = \mathbf{u}^0 + r\mathbf{s}^1 \quad (5.16)$$

An initial point $\mathbf{b}^1 = \mathbf{u}(r^*)$ on the constant orientation workspace boundary

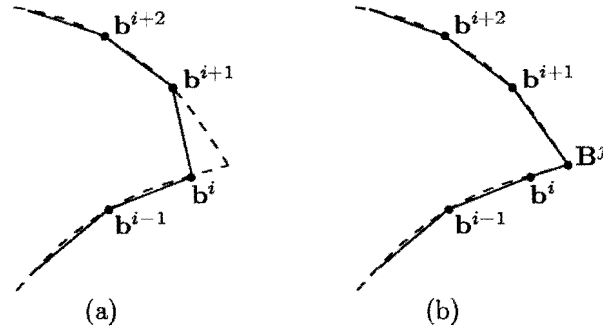


Figure 5.2: The importance of mapping bifurcation points

the two active constraints. This can be easily accomplished by solving the following least squares optimization problem:

$$\min_{\mathbf{u}} \|\mathbf{p}(\mathbf{u}, w^{\text{fix}}) - \mathbf{p}^{\text{ext}}\|^2 \quad (5.20)$$

where \mathbf{p} contains the active set of constraints from (5.3) or (5.4) and \mathbf{p}^{ext} the corresponding upper or lower limits. Active constraints, and the presence of bifurcation points can be determined by continuously monitoring the values of constraints (5.3) or (5.4) while tracing the workspace boundary. Figure 5.2 illustrates the importance of mapping bifurcation points. Successive points determined along the workspace boundary ∂W^C using the chord method are $\mathbf{b}^{i-1}, \dots, \mathbf{b}^{i+2}$. It is evident on comparison of Figure 5.2 (a) and (b) that the inclusion of the bifurcation point \mathbf{B}^j results in a much more accurate representation of the workspace boundary.

5.5 Dextrous workspace determination

This section presents a new numerical multi-level optimization methodology for determining dextrous workspaces of planar parallel manipulators. The methodology is based on the chord method discussed in Appendix C, which was extended and refined in the previous section for determining constant orientation workspaces. It should be noted that the method proposed here

differs from the optimization method for determining dextrous workspaces proposed by Du Plessis and Snyman [18]).

5.5.1 Workspace definitions

Dextrous workspace

The dextrous requirement for the manipulator at a point \mathbf{u} is that all orientations in the range

$$\phi^{\min} \leq w \leq \phi^{\max} \quad (5.21)$$

can be attained by the manipulator (see Section 1.3.1). The dextrous workspace $W^D[\phi^{\min}, \phi^{\max}]$ of the planar manipulator is thus defined as:

$$W^D = \{\mathbf{u} \in \mathfrak{R}^{nu} : \Phi(\mathbf{u}, \mathbf{v}, w) = \mathbf{0}, \text{ with } \mathbf{v} \text{ satisfying (5.3)} \quad (5.22)$$

$$\text{and } \mathbf{g}(\mathbf{u}, \mathbf{v}, w) \text{ satisfying (5.4) for all } w \in [\phi^{\min}, \phi^{\max}]\}$$

The boundary ∂W^D of the dextrous workspace can thus be defined as:

$$\partial W^D = \{\mathbf{u} \in \mathfrak{R}^{nu} : \mathbf{u} \in W^D \text{ and } \exists \text{ an } \mathbf{s} \in R^{nu} \text{ such that for} \quad (5.23)$$

$$\mathbf{u}' = \mathbf{u} + \lambda \mathbf{s}, \lambda \in \mathfrak{R} \text{ arbitrarily small and either positive}$$

$$\text{or negative, no } \mathbf{v} \text{ exists that satisfies } \Phi(\mathbf{u}', \mathbf{v}, w) = \mathbf{0};$$

$$\text{as well as inequalities (5.3) and (5.4) for all } w \in [\phi^{\min}, \phi^{\max}]\}$$

In order to calculate the dextrous workspace, it is necessary to be able to calculate the manipulator orientation workspace, for any given position \mathbf{u} , as well.

Orientation workspace

The orientation workspace $W^O[\mathbf{u}^{\text{fix}}]$ of a manipulator, for a fixed position \mathbf{u}^{fix} of the working point, is the set of orientations that can be attained by the

manipulator end-effector (see Section 1.3.1). For a planar manipulator, since only one rotation is possible (about the z -axis perpendicular to the plane), the orientation workspace is one-dimensional and can easily be specified by the maximum w^{\max} and minimum w^{\min} orientations attainable by the manipulator end-effector. For a given \mathbf{u}^{fix} , the orientation workspace can thus be described mathematically as

$$W^O[\mathbf{u}^{\text{fix}}] = \{w \in \mathfrak{R} : \Phi(\mathbf{u}^{\text{fix}}, \mathbf{v}, w) = \mathbf{0} \text{ with } \mathbf{v} \text{ satisfying (5.24)} \\ \text{(5.3) and } \mathbf{g}(\mathbf{u}^{\text{fix}}, \mathbf{v}, w) \text{ satisfying (5.4)}\}$$

The boundary ∂W^O of the orientation workspace for a planar manipulator is thus

$$\partial W^O[\mathbf{u}^{\text{fix}}] = \{w \in O \text{ and } \exists \text{ a } \lambda \in \mathfrak{R} \text{ such that for } w' = w + \lambda \\ \text{with } \lambda \text{ arbitrarily small and either positive or (5.25)} \\ \text{negative, no } \mathbf{v} \text{ exists that satisfies } \Phi(\mathbf{u}^{\text{fix}}, \mathbf{v}, w') = \mathbf{0} \\ \text{as well as conditions (5.3) and (5.4)}\}$$

In practical terms, for \mathbf{u}^{fix} , the values of w^{\min} and w^{\max} may easily be obtained numerically by solution of the following optimization problem.

$$\max_w (w - w^{\text{ave}})^2 \\ \text{subject to } \mathbf{v}^{\min} \leq \mathbf{v}(\mathbf{u}^{\text{fix}}, w) \leq \mathbf{v}^{\max}, \quad (5.26) \\ \mathbf{g}^{\min} \leq \mathbf{g}(\mathbf{u}^{\text{fix}}, \mathbf{v}, w) \leq \mathbf{g}^{\max}$$

where w^{ave} is a suitably chosen value of the manipulator orientation that lies inside the orientation workspace. By choosing a suitable starting point for optimization problem (5.26) the values of w^{\min} and w^{\max} , corresponding to the two extreme local minima, can be determined.

5.5.2 Mapping the dextrous workspace boundary

Finding an initial point on the workspace boundary

Finding an initial point on the dextrous workspace boundary requires the sequential solution of three problems:

1. Finding the assembled point \mathbf{u}^a of the manipulator with input coordinates at their average value.
2. Finding the point \mathbf{u}^d where the manipulator has its greatest dextrous ability.
3. Determining an initial point \mathbf{b}^1 on the dextrous workspace boundary.

These three steps are realized through the implementation of three different constrained optimization problems, which result in a reliable and automatic determination of the initial boundary point \mathbf{b}^1 .

Step 1 essentially involves the solution of the forward kinematics of the manipulator, i.e. solve for \mathbf{u} and w in (5.2) with \mathbf{v} prescribed as

$$\bar{\mathbf{v}} = (\mathbf{v}^{\min} + \mathbf{v}^{\max})/2 \quad (5.27)$$

In practice this can be done by solving the least squares optimization problem

$$\min_{\mathbf{u}, w} \|\mathbf{v}(\mathbf{u}, w) - \bar{\mathbf{v}}\|^2 \quad (5.28)$$

where $\mathbf{v}(\mathbf{u}, w)$ denotes the inverse kinematic solution of (5.2) for any given \mathbf{u} and w . The solution of this problem yields the correct value for \mathbf{u}^a .

The point of greatest dexterity of the manipulator \mathbf{u}^d (Step 2) can similarly be determined by means of the unconstrained optimization problem:

$$\max_{\mathbf{u}} (w^{\max}(\mathbf{u}) - w^{\min}(\mathbf{u}))^2 \quad (5.29)$$

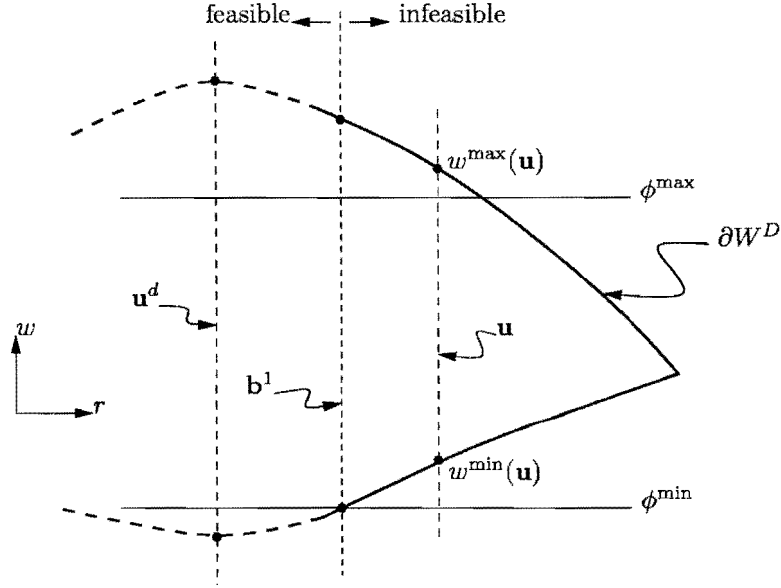


Figure 5.3: Finding an initial point on the dextrous workspace boundary

where the values of $w^{\min}(\mathbf{u})$ and $w^{\max}(\mathbf{u})$ for a fixed \mathbf{u} , are determined by solution of optimization problem (5.26), i.e. by determining the orientation workspace of the manipulator at point \mathbf{u} .

Consistent with the definition of ∂W^D in (5.23), an initial point \mathbf{b}^1 on the dextrous workspace boundary in an arbitrary direction from \mathbf{u}^d , designated by a unit vector $\mathbf{s}^1 \in \mathbb{R}^{n_u}$, is determined by solving the following constrained optimization problem (corresponding to optimization problem (C.9) in Appendix C):

$$\begin{aligned} & \max_r r^2 \\ & \text{such that } c_1 = \phi^{\max} - w^{\max}(\mathbf{u}(r)) \leq 0; \\ & c_2 = w^{\min}(\mathbf{u}(r)) - \phi^{\min} \leq 0 \end{aligned} \quad (5.30)$$

where $\mathbf{u}(r) = \mathbf{u}^d + r\mathbf{s}^1$. The solution of this problem is schematically illustrated in Figure 5.3. Once more the the values of $w^{\min}(\mathbf{u})$ and $w^{\max}(\mathbf{u})$ for a point \mathbf{u} in (5.30), are determined by solution of optimization problem (5.26).

Mapping the workspace boundary

Once an initial point on the workspace boundary has been found, subsequent points can be mapped using the chord methodology. The updated form of optimization problem (C.12) is

$$\begin{aligned} & \min_{\omega} \omega^2 \\ \text{such that } & c_1 = \phi^{\max} - w^{\max}(\mathbf{u}(\omega)) \leq 0; \\ & c_2 = w^{\min}(\mathbf{u}(\omega)) - \phi^{\min} \leq 0 \end{aligned} \quad (5.31)$$

where $\mathbf{u}(\omega)$ is as defined in (5.18), and w^{\min} and w^{\max} are determined using optimization problem (5.26), hence the description of the methodology as multi-level. The basic form of the chord methodology remains otherwise the same as described in Appendix C.

5.5.3 Determination of bifurcation points

It is evident that any point on the dextrous workspace boundary will be associated with either a maximum ϕ^{\max} or minimum ϕ^{\min} orientation of the manipulator (see Figure 5.3). In addition, since the solution to optimization problem (5.26) is implicit in solving (5.31), each boundary point is also associated with an extreme leg value. In fact, the workspace boundary is associated with a number of curves, each corresponding to a different extreme leg value and associated extreme platform orientation. Points where these curves meet are termed *bifurcation points* since the manipulator may assume one of two distinct extreme states when travelling clockwise or counter-clockwise along the workspace boundary from such a point. When determining the dextrous workspace, a distinction must be made between two different types of bifurcation points.

Type I bifurcation points

Type I bifurcation points occur along the workspace boundary when two intersecting boundary curves are both associated with the *same* extreme orientation, either ϕ^{\min} or ϕ^{\max} of the platform. Each curve will additionally be associated with one leg at an extreme length. In the vicinity of the intersection, the precisely active leg, and associated active boundary curve, can be determined by examination of the final values of the constraints from optimization problem (5.31). In this way, at the intersection or bifurcation point, two legs m and n will both be at known extreme values v_m^{ext} and v_n^{ext} , and the platform will be at a known extreme orientation ϕ^{ext} . We need then to simply solve the inverse kinematics to determine the exact coordinates of the type I bifurcation point \mathbf{B}^j . This is done by the solution of the following optimization problem:

$$\min_{\mathbf{u}} (v_m(\mathbf{u}, \phi^{\text{ext}}) - v_m^{\text{ext}})^2 + (v_n(\mathbf{u}, \phi^{\text{ext}}) - v_n^{\text{ext}})^2 \quad (5.32)$$

which will yield the coordinates of the bifurcation point.

Type II bifurcation points

Type II bifurcation points are associated with a change in the active extreme orientation of the platform. Thus at these points the maximum w^{\max} and minimum w^{\min} values of platform orientation will both simultaneously be exactly equal to the maximum and minimum prescribed orientation values ϕ^{\max} and ϕ^{\min} . Therefore to determine such points, constraints c_1 and c_2 given in equations (5.30) and (5.31) must both be *exactly* satisfied. This may be accomplished by solving the following unconstrained optimization problem:

$$\min_{\mathbf{u}} \{ (\phi^{\max} - w^{\max}(\mathbf{u}))^2 + (\phi^{\min} - w^{\min}(\mathbf{u}))^2 \} \quad (5.33)$$

The complete multi-level optimization algorithm for dextrous workspace determination is summarized in Algorithm 5.1.



Algorithm 5.1 Dextrous workspace determination

1. Determine the assembled point \mathbf{u}^a of the mechanism using optimization problem (5.28).
 2. Determine the point of greatest dexterity \mathbf{u}^d using optimization problem (5.29).
 3. Determine an initial point on the workspace boundary by means of optimization problem (5.30).
 4. Using optimization problem (5.31), determine successive points along the boundary at chord intervals d . Identify and map type I and II bifurcation points as they occur using either optimization problem (5.32) or (5.33).
 5. Terminate when condition (C.14) becomes true or when the specified maximum number of iterations is exceeded.
-

	x_C	y_C	x_D	x_E	r
M1	-1	0	1	2	1
M2	-0.75	0	0.75	1.5	0.75
M2	-0.5	0	0.5	1	0.25

Table 5.1: Geometric parameters for manipulator designs M1-M3

5.5.4 Numerical results

Three different manipulator geometries, denoted M1-M3 are used in illustrating the proposed methodology. The three sets of five parameters defining the three different manipulator designs are given in Table 5.1. Extreme leg lengths for the manipulators considered here are $l_1^{\min} = l_2^{\min} = \sqrt{2}$, $l_3^{\min} = 1$, $l_1^{\max}, l_2^{\max} = 2$, $l_3^{\max} = \sqrt{3}$. The chord algorithm described in Algorithm 5.1, implemented in FORTRAN on a 1.6 GHz Pentium 4 computer, was applied in determining the various dextrous workspaces of these manipulators. The dextrous workspaces were obtained for various ranges of dexterity and are given in Figures 5.4 to 5.6. For the various dextrous workspaces obtained, Table 5.2 gives the number of points determined on each workspace boundary n_b , as well as the computational time t required for computing each dextrous workspace. Investigation of the performance of the algorithm has revealed that a large portion of the computational cost is related to solving optimization problem (5.26), to determine the manipulator orientation workspaces. In many cases, it may be possible to determine such orientation workspaces analytically, which would dramatically reduce the time needed to compute the dextrous workspace. Here though, the numerical approach has been presented since it provides an alternative, generally applicable methodology.

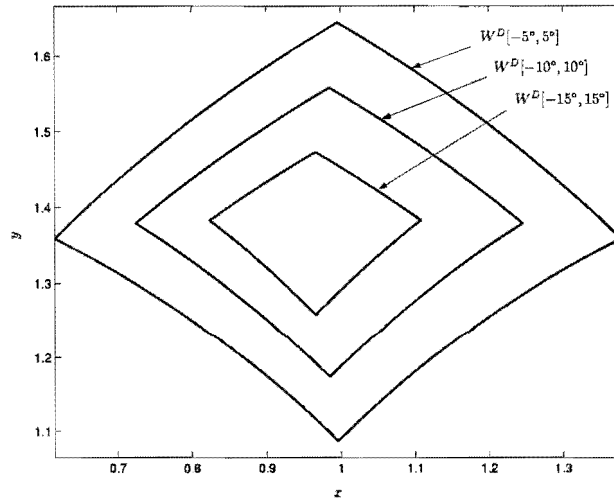


Figure 5.4: Dextrous workspaces of M1

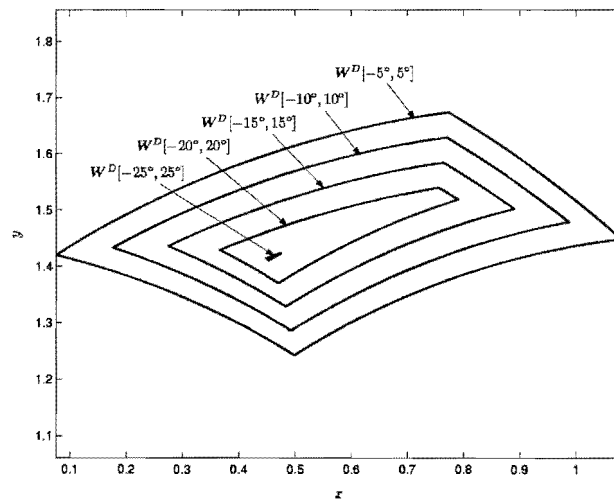


Figure 5.5: Dextrous workspaces of M2

5.6 Optimization for a single prescribed constant orientation workspace

The constrained optimization methodology developed in Section 4.7 is applied here to the 3-dof manipulator in the following form:

SO synthesis: *Determine a manipulator design that reaches, with optimal conditioning, a prescribed constant orientation workspace.*

5.6.1 Optimization formulation

As in Section 4.5.1, the prescribed workspace is defined by polar coordinates (β_p, r_p) centered on a local coordinate system $x' - y'$ at \mathbf{O}' . The boundary of the constant workspace $W_c^C[\phi^{\text{fix}}]$ associated with design \mathbf{d} is represented in a similar manner (refer to Figure 4.2). The chord method (see Section 5.4) is used to generate points \mathbf{b}_c^i , with corresponding polar coordinates (β_c^i, r_c^i) , on the constant orientation workspace boundary.

Dropping the $[\phi^{\text{fix}}]$, which is implicit when referring to constant orientation workspaces W^C for the rest of this section, the part of the prescribed workspace W_p^C not intersecting calculated workspace W_c^C is denoted δW_p^C , and the part of workspace W_c^C not intersecting W_p^C is denoted δW_c^C . The calculation of approximations to the areas δW_p^C and δW_c^C is performed using the numerical scheme described in Section 4.5.1.

SO synthesis is thus achieved by solution of the following optimization prob-

lem:

$$\begin{aligned} & \max_{\mathbf{d}} \left\{ \min_{\mathbf{u} \in W_p^C[\phi^{\text{fix}}]} \kappa^{-1}(\mathbf{d}, \mathbf{u}) \right\} \\ & \text{subject to the inequality constraint} \\ & g(\mathbf{d}) \leq 0 \end{aligned} \quad (5.34)$$

where the intermediate coordinate $w = \phi^{\text{fix}}$ is prescribed and fixed, and where the inequality constraint function $g(\mathbf{d})$ is defined as

$$g(\mathbf{d}) = \begin{cases} \delta W_p^C & \text{if } \delta W_p^C > 0 \\ -r^2 & \text{if } \delta W_p^C = 0 \end{cases} \quad (5.35)$$

where r is calculated as before (see Section 4.7). The solution to optimization problem (5.34) seeks to improve the *single worst point* with respect to chosen performance measure, κ^{-1} , within the *prescribed* workspace, W_p^C .

Once again the question of how to determine the smallest value of κ^{-1} over the set $\mathbf{u} \in W_p^C$ arises. It has been shown for the planar 2-dof manipulator, that the maximum value of κ (or minimum of κ^{-1}) will lie on the boundary ∂W_p^C of the prescribed workspace (See Appendix D). An assumption is made that a similar result can be found for the particular 3-dof manipulator to be investigated here. The minimum value of the inverse condition number κ^{-1} can thus be approximated by calculating κ^{-1} at points \mathbf{b}_p^i , $i = 1, \dots, n_{bc}$ simultaneously to the determination of the boundary points \mathbf{b}_c^i , $i = 1, \dots, n_{bc}$. The overall minimum of the κ^{-1} values at these candidate points may then easily be determined. Based on the results presented throughout this chapter it appears that the above assumption is valid.

5.6.2 Numerical results

The method described above, and embodied by optimization problem (5.34), has been applied to the 3-dof planar parallel manipulator for three different prescribed workspaces. These prescribed workspaces are centered at $\mathbf{O}' =$

	N^g	$f(\mathbf{d}^0)$	f^*	g^*	\mathbf{d}^*
P1	21	0.759	0.912	$0.2E - 5$	$[-1.111, 0.2317, 1.277, 1.967, 0.9159]^\top$
P2	17	0.768	0.927	$0.4E - 9$	$[-1.153, 0.3003, 1.275, 1.906, 0.9401]^\top$
P3	71	0.747	0.943	$0.1E - 4$	$[-1.170, 0.3365, 1.463, 1.946, 0.9108]^\top$

Table 5.3: SO synthesis solutions

$[1, 1.5]^\top$. They are chosen to correspond to workspaces P1-P3 in Section 4.7, scaled down by a factor of 5 for workspaces P1 and P2 and by 7 for P3. This was done so that the prescribed workspaces were of such diameter that feasible solutions for the choice of actuator leg lengths existed. It is assumed the actuators have been chosen and thus that the maximum and minimum leg lengths are predetermined. The remaining five design variables for the problem are thus

$$\mathbf{d} = [x_C, y_C, x_D, x_E, r]^\top \quad (5.36)$$

Actuator limits were chosen as $l_i^{\min} = \sqrt{2}$, $l_i^{\max} = 2$, $i = 1, 2$ and $l_3^{\min} = 1$, $l_3^{\max} = \sqrt{3}$. Actuator leg lengths and the initial design vector $\mathbf{d}^0 = [-1, 0, 1, 2, 1]^\top$ were selected to correspond to the manipulator studied by Haug *et al.* [16].

The prescribed workspaces P1-P3, the workspace corresponding to the initial design vector and inverse condition number contours for this startign design are shown in Figure 5.7(a). The Dynamic-Q optimization algorithm (see Chapter 3) was used to perform the optimization with move limit $\rho = 0.1$, termination parameters $\varepsilon_f = 10^{-6}$ and $\varepsilon_x = 10^{-4}$, and a finite difference interval $\Gamma = 10^{-6}$ for calculating the gradients of the optimization functions. The chord length for calculating the workspace was $d = 0.02$. For all manipulators the orientation of the platform was fixed at $\phi_P = 0^\circ$.

Numerical results for each of the runs from the starting point \mathbf{d}^0 and for the different prescribed workspaces are reported in Table 5.3, which gives the number of gradient evaluations N^g required for convergence, the initial

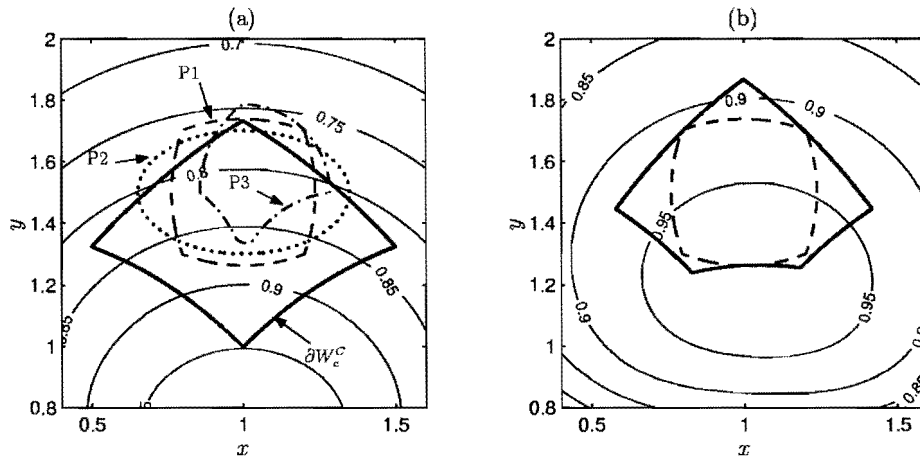


Figure 5.7: SO synthesis (a) prescribed workspaces P1-P3, manipulator workspace and corresponding κ^{-1} contours corresponding to the starting design and (b) prescribed workspace P1 and corresponding optimal manipulator workspace and κ^{-1} contours

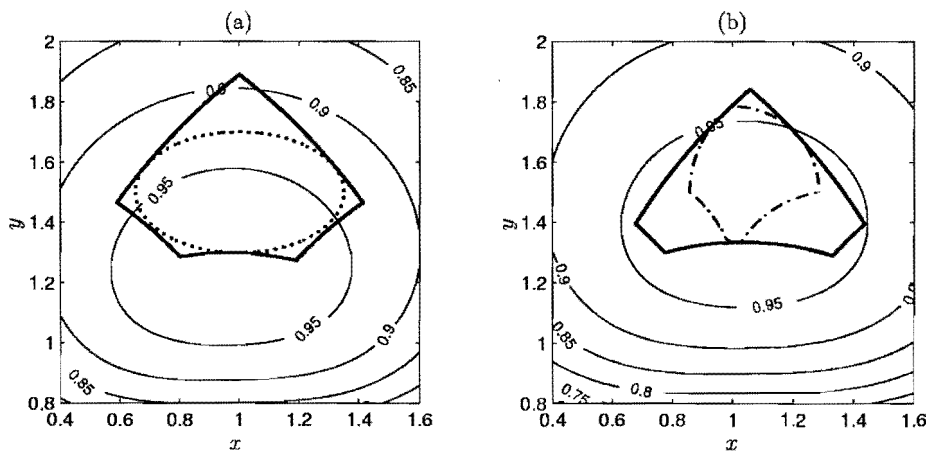


Figure 5.8: SO synthesis manipulator workspace and κ^{-1} contours corresponding to the optimal design for prescribed workspaces (a) P2 and (b) P3

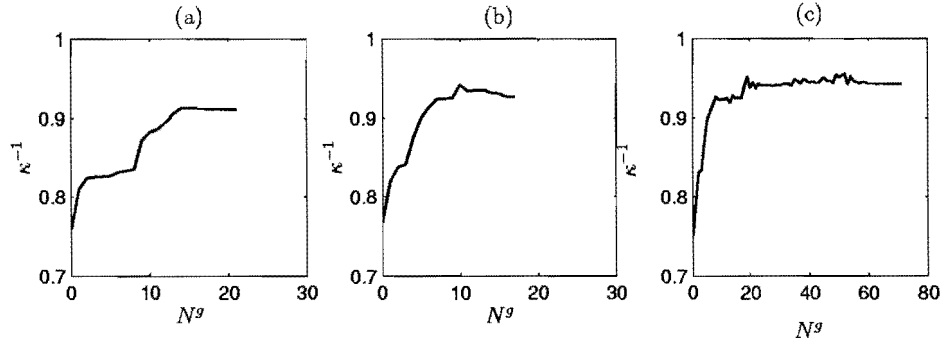


Figure 5.9: SO synthesis convergence histories for (a) P1, (b) P2 and (c) P3

function value $f(\mathbf{d}^0)$, converged objective function value f^* , corresponding inequality constraint function value g^* and components of the optimum design vector \mathbf{d}^* . The resultant workspaces and inverse condition number contours corresponding to P1-P3 are shown in Figure 5.7(c) and Figure 5.8(a) and (b) respectively. Finally Figure 5.9 gives the convergence histories for the various prescribed workspaces.

5.7 Optimization for multiple prescribed constant orientation workspaces

MO synthesis: *Determine a manipulator design that reaches, with optimal conditioning, multiple prescribed constant orientation workspaces.*

5.7.1 Optimization formulation

Some strategy needs to be implemented for dealing with the orientational capability of the manipulator. This point is addressed by evaluating the SO optimization problem of the previous section at various angular “slices”

through the workspace. This is the approach used by Boudreau and Gosselin [86] in an unconstrained case. Accordingly, in the methodology proposed here, the minimization over $\mathbf{u} = [x, y]^T$ in (5.34) is carried out, not only for a *single* prescribed value of ϕ_P , but over *multiple* slices of the prescribed workspace corresponding to m^{sl} fixed values of ϕ_P . For illustration of the methodology in this section $m^{\text{sl}} = 3$ with slices through the workspace at $\phi_P = \phi^{\text{min}}, \phi^{\text{int}}, \phi^{\text{max}}$. In solving the MO optimization problem the resulting design is expected to fulfil the dexterity requirement of operating over the range of $\phi_P = [\phi^{\text{min}}, \phi^{\text{max}}]$ within the prescribed workspace.

Optimization problem (5.34), modified to allow for optimization over the three values ($m^{\text{sl}} = 3$) of $w = \phi_P$, becomes

$$\begin{aligned} \max_{\mathbf{d}} \left\{ \min_{\mathbf{u} \in W_p^C[\phi^i], i=1, \dots, m^{\text{sl}}} \kappa^{-1}(\mathbf{d}, \mathbf{u}) \right\} \\ \text{subject to the inequality constraint} \\ g(\mathbf{d}) \leq 0 \end{aligned} \quad (5.37)$$

The inequality constraint function is defined as follows:

$$g(\mathbf{d}) = \begin{cases} S = \sum_{i=1}^{m^{\text{sl}}} \delta W_p^C[\phi^i], i = 1, \dots, m^{\text{sl}} & \text{if } S > 0 \\ -r^2 & \text{if } S = 0 \end{cases} \quad (5.38)$$

5.7.2 Numerical results

The prescribed workspaces P1-P3, corresponding to those used in Section 5.6, are shown in Figure 5.10. The manipulator workspaces corresponding to an initial design vector $\mathbf{d}^0 = [-0.75, 0, 0.75, 1.5, 0.75]^T$ for the various constant orientations, as well as the corresponding inverse condition number contours are shown in the same figure. Actuator limits were again chosen as $l_i^{\text{min}} = \sqrt{2}$, $l_i^{\text{max}} = 2, i = 1, 2$ and $l_3^{\text{min}} = 1, l_3^{\text{max}} = \sqrt{3}$. The constant orientation slices through the workspace were made at $\phi_P = -5^\circ, 0^\circ, +5^\circ$. Figure 5.10 clearly

	N^g	$f(\mathbf{d}^0)$	f^*	g^*	\mathbf{d}^*
P1	33	0.677	0.901	$0.2E - 5$	$[-1.034, 0.2484, 1.331, 1.657, 0.8553]^T$
P2	25	0.681	0.917	$0.1E - 4$	$[-1.061, 0.2721, 1.345, 1.718, 0.861]^T$
P3	44	0.666	0.915	$0.1E - 4$	$[-1.072, 0.3103, 1.420, 1.621, 0.8778]^T$

Table 5.4: MO synthesis solutions

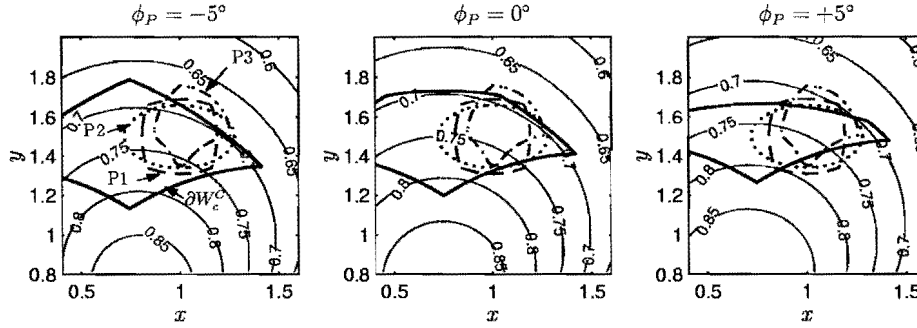


Figure 5.10: MO synthesis prescribed workspaces P1-P3 and manipulator workspace and κ^{-1} contours corresponding to the starting design

shows that the initial design \mathbf{d}^0 is infeasible because for each orientational slice the prescribed workspace is not contained in the reachable workspace. The Dynamic-Q optimization algorithm move limit used was $\rho = 0.1$ and the chord length for calculating the workspace was $d = 0.02$. Convergence tolerances used for Dynamic-Q were $\varepsilon_x = 10^{-4}$ and $\varepsilon_f = 10^{-5}$ and a finite difference of $\Gamma = 10^{-6}$ was used for calculating function gradients.

The workspaces, and κ^{-1} contours corresponding to the optimal designs for prescribed workspaces P1-P3 are shown in Figures 5.11 to 5.13. Table 5.4 summarizes the number of gradient evaluations N^g required for convergence, the initial $f(\mathbf{d}^0)$ and final f^* objective function values, inequality constraint function value at convergence c^* and optimal design \mathbf{d}^* for each prescribed workspace. Figure 5.14 shows the convergence histories for the various optimization runs.

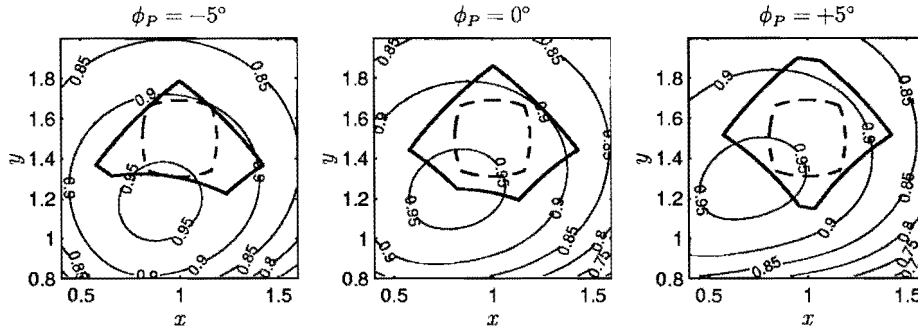


Figure 5.11: MO synthesis manipulator workspace and κ^{-1} contours corresponding to the optimal design for prescribed workspace P1

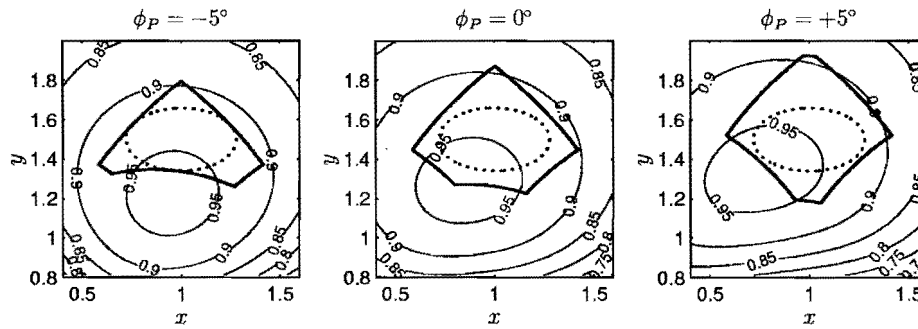


Figure 5.12: MO synthesis manipulator workspace and κ^{-1} contours corresponding to the optimal design for prescribed workspace P2

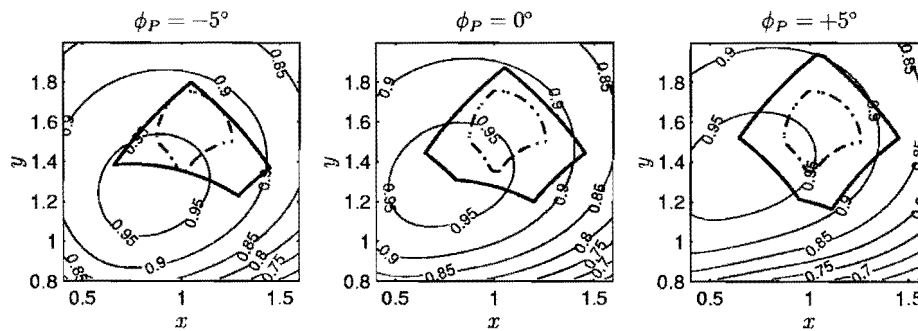


Figure 5.13: MO synthesis manipulator workspace and κ^{-1} contours corresponding to the optimal design for prescribed workspace P3

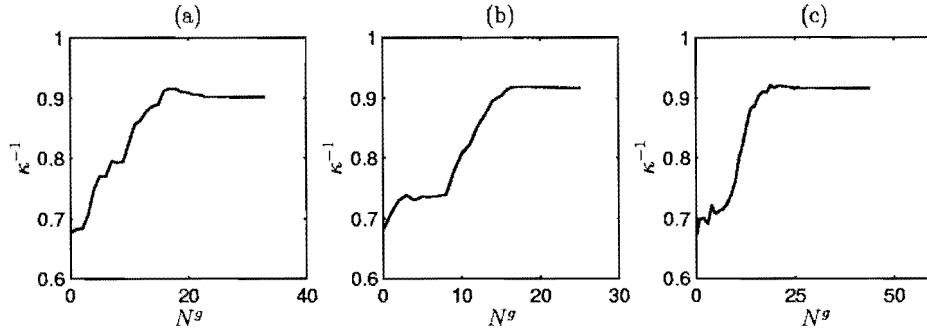


Figure 5.14: MO synthesis convergence histories for (a) P1, (b) P2 and (c) P3

5.8 Optimization for a prescribed dextrous workspace

D synthesis: *Determine a manipulator design that reaches, with optimal conditioning, a prescribed [continuous] dextrous workspace.*

5.8.1 Optimization formulation

Using the methodology for determining dextrous workspaces developed in Section 5.5, the planar parallel manipulator can, as an alternative to MO methodology, be directly synthesized for a prescribed dextrous workspace and optimal conditioning. The form of the optimization problem for achieving this is

$$\begin{aligned} & \max_{\mathbf{d}} \left\{ \min_{\mathbf{u} \in W_p^C[\phi^{\min}], W_p^C[\phi^{\max}]} \kappa^{-1}(\mathbf{d}, \mathbf{u}) \right\} \\ & \text{subject to the inequality constraint} \\ & g(\mathbf{d}) \leq 0 \end{aligned} \quad (5.39)$$

where the inequality constraint function is defined as follows:

$$g(\mathbf{d}) = \begin{cases} \delta W_p^D[\phi^{\min}, \phi^{\max}] & \text{if } \delta W_p^D[\phi^{\min}, \phi^{\max}] > 0 \\ -r^2 & \text{if } \delta W_p^D[\phi^{\min}, \phi^{\max}] = 0 \end{cases} \quad (5.40)$$

The minimum value of the condition number is determined using the same approach as given in Section 5.6. Once again it is assumed that the minimum value of κ^{-1} occurs on the boundary of the prescribed workspace. Furthermore it is expected, based on the results obtained in Section 5.7, that the minimum value will also be associated with an extreme platform orientation, ϕ^{\min} or ϕ^{\max} . Thus in determining the minimum value of κ^{-1} over $W_p^D[\phi^{\min}, \phi^{\max}]$, only the workspace boundaries of $W_p^C[\phi^{\min}]$ and $W_p^C[\phi^{\max}]$, corresponding to the “edges” of the prescribed dextrous workspace, are considered. These assumptions appear to be valid, based on the results obtained here.

5.8.2 Numerical results

The optimization problem embodied in (5.39) has been implemented, once more using the Dynamic-Q algorithm to find optimal designs for prescribed workspace P1-P3. Parameters used for Dynamic-Q were convergence tolerances $\varepsilon_x = 10^{-4}$ and $\varepsilon_f = 10^{-6}$ and a move limit $\rho = 0.05$. Gradients were calculated using *central differences* and a finite difference interval of $\Gamma = 10^{-3}$. A chord length of $d = 0.02$ was used for all calculations. Results obtained are summarized in Figures 5.15 and 5.16 and Table 5.5. The various quantities given in Table 5.5 are the same as those given in Table 5.4.

Comparison of these results with those given for the MO synthesis in Section 5.7.2 indicates that, in general, $f_D^* \leq f_{MO}^*$. This is to be expected, since the specification of a prescribed *dextrous* workspace places a more stringent requirement on the numerical optimization, resulting in lower optimal objective function values in these cases.

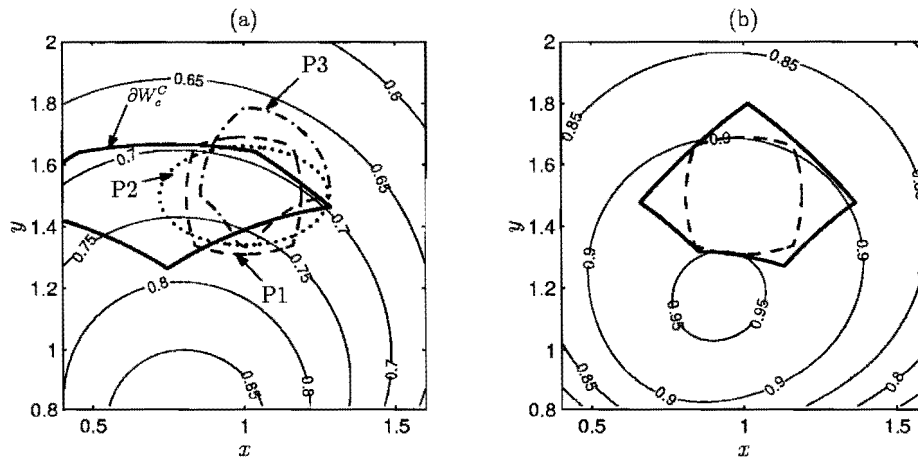


Figure 5.15: D synthesis (a) prescribed workspaces P1-P3, manipulator workspace and corresponding κ^{-1} contours corresponding to the starting design and (b) prescribed workspace P1 and corresponding optimal manipulator workspace and κ^{-1} contours

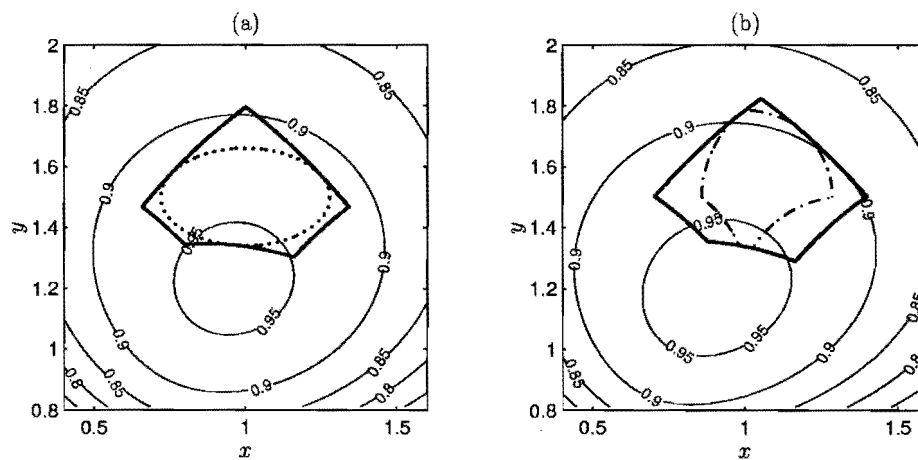


Figure 5.16: D synthesis manipulator workspace and κ^{-1} contours corresponding to the optimal design for prescribed workspaces (a) P2 and (b) P3

	N^g	$f(\mathbf{d}^0)$	f^*	g^*	\mathbf{d}^*
P1	33	0.677	0.897	$0.2E-5$	$[-0.9884, 0.2466, 1.339, 1.664, 0.8413]^T$
P2	36	0.681	0.916	$0.6E-7$	$[-1.050, 0.2717, 1.356, 1.716, 0.8500]^T$
P3	52	0.660	0.892	$0.1E-4$	$[-0.9890, 0.2816, 1.362, 1.668, 0.8678]^T$

Table 5.5: D synthesis solutions

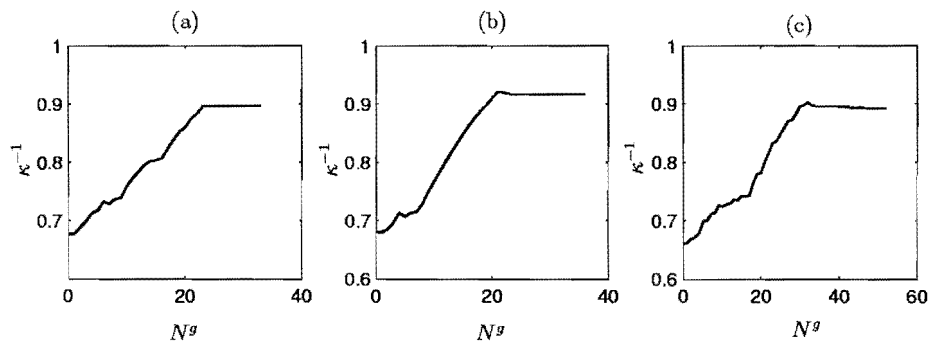


Figure 5.17: D synthesis convergence histories for (a) P1, (b) P2 and (c) P3

5.9 Conclusion

The chord workspace determination methodology, as proposed at the start of this chapter, for the determination of constant orientation and dextrous workspaces, is a reliable and efficient numerical methodology. This has been proven by the fact that optimization of the 3-dof manipulators in the latter part of the chapter inherently requires many manipulator workspaces evaluations, which have been performed robustly by the chord method.

For the 3-dof manipulator studied here the dimensional synthesis results obtained are encouraging, optimum solutions having been obtained with minimal computational effort compared to that which would have been required using evolutionary optimization algorithms. For each of the three synthesis methodologies presented, not only are manipulator dimensions determined so that the prescribed workspace can be reached by the manipulator, but also so that the inverse condition number is as high as possible throughout the prescribed workspace. The proposed methodology produces convincing results, indicating it to be a stable and efficient numerical method for designing planar parallel manipulators. The Dynamic-Q optimization algorithm used in the synthesis methodology exhibits high efficiency in solving the associated optimization problem.